# Shadows and photon motions in the axially symmetric Finslerian extension of a Schwarzschild black hole

Ke-Jian He,[1,†] Jin-Tao Yao,[1,‡] Xiao Zhang,[2,§] and Xin Li[1,*]

[1]*Department of Physics and Chongqing Key Laboratory for Strongly Coupled Physics, Chongqing University, Chongqing 401331, China*

[2]*Hongshen Honors School, Chongqing University, Chongqing 401331, China*

(Received 25 December 2023; accepted 23 February 2024; published 15 March 2024)

In this paper, we have conducted a thorough investigation into the shadow characteristics exhibited by the axially symmetric Finslerian extension of a Schwarzschild black hole and supplementary numerically simulated the motion behavior of photons near the black hole with respect to varying Finsler parameter $\epsilon$ and observation inclinations $\theta_o$. In this spacetime, the apparent shape and size of the black hole shadow remain the same as the one in the Schwarzschild black hole, regardless of changes in the Finsler parameter $\epsilon$. However, the apparent position of shadow in the observer's sky plane appears to shift along the horizontal axis, and the distance moved is positively correlated with the value of the Finsler parameter $\epsilon$. Interestingly, with a fixed value of $\epsilon$, the displacement of the visual position of shadow is rectified as the observation angle decreases. In addition, it is demonstrated that the motion behavior of photons around the axially symmetric Finslerian extension of a Schwarzschild black hole has a greater degree of deflection than a Schwarzschild black hole, although their shadows are in some cases consistent in shape, size, and apparent position. These results can serve as a valuable tool in distinguishing the axially symmetric Finslerian extension of a Schwarzschild black hole from its counterparts in general relativity.

DOI: 10.1103/PhysRevD.109.064049

## I. INTRODUCTION

After formulating the theory of general relativity (GR), Einstein postulated the existence of immensely compact celestial objects in our Universe, specifically the black hole. It is a region of spacetime with an incredibly potent gravitational field, whereby any matter that crosses its event horizon, including light, will be inexorably drawn into it. In 1965, the presence of a black hole was confirmed by the theoretical calculation of Penrose [1]. In 2015, the Laser Interferometer Gravitational Wave Observatory (LIGO) detected the gravitational wave signal, resulting from the merger of two black holes, signifying a groundbreaking moment in human history as the existence of black holes is confirmed [2–4]. In a landmark achievement, the Event Horizon Telescope Collaboration (EHT) unveiled images of the black hole situated at the core of radio galaxy M87* [5–10] and that of Milky Way's center Sagittarius A* [11–16], providing an unprecedented glimpse into these mysterious celestial objects. Consequently, human exploration of the Universe and its enigmatic black holes has entered a novel epoch.

One of the most intriguing aspects of black holes is the shadow, which has been a subject of extensive research over time. The initial theoretical introduction regarding the black hole shadow was proposed by Synge, who demonstrated that the shadow of a spherically symmetric black hole is a standard circle, thereby implying that the angular diameter of the shadow can be expressed as a function of the black hole mass and the radius coordinates of the observer's position [17]. Subsequently, Bardeen utilized the notion of a critical curve to delineate the shadow of the black hole, namely the inner region of a critical curve, and obtained the radius of the shadow of a Schwarzschild black hole $r = 3\sqrt{3}M$ ($M$ is the mass of the black hole) [18,19]. For the Kerr black hole, an observer located on the axis of rotation would still perceive the black hole shadow as a circular void, while an observer situated on the equatorial plane would witness a gradual transformation of the shadow from a disklike shape to that resembling a $D$ shape with increasing values of the rotation parameter. When investigating the shadow of a phantom black hole and considering the circumstances in which photons are coupled to the Weyl tensor, Huang *et al.* discovered that the coupling will cause photons with different polarization directions to travel along different paths, resulting in a double shadow of a black hole [20]. Through the study of black hole shadows with mass vector fields, Cunha *et al.* have discovered that the shadow presents a novel conical

*Corresponding author: lixin1981@cqu.edu.cn
†kjhephys@cqu.edu.cn
‡yaojintao@stu.cqu.edu.cn
§xzhangphysik@cqu.edu.cn

 

shadow in the case of specific parameters [21]. In [22], Wang *et al.* investigated the shadow of the Konoplya-Zhidenko rotating black hole and derived conditions for the emergence of the $D$ shape and conical shadows. Certainly, extensive research has been conducted on the impact of varying observer positions on the profile of a black hole shadow [23]. In addition, the researches on black hole shadow have achieved a number of significant progress, such as the black hole event horizon, the photon sphere and the shadow radius meet a series of inequalities [24], the relevant parameters of the black hole can be extracted through the shadow radius [25], among other findings can be referred to [26–34].

The investigation of black hole shadows not only uncovers the fundamental characteristics of black holes, but also serves as an effective means to probe the characteristics of spacetime. Currently, most theoretical investigations into black hole shadows are situated within the framework of the theory of general relativity or various modified theories of gravity, with adopting Riemannian geometry as their background. Finsler geometry, a natural extension of Riemannian geometry, is commonly acknowledged as a type of Riemannian geometry that does not impose the quadratic constraints [35]. Hence, Finsler geometry encompasses Riemannian geometry as a special case and offers higher degrees of freedom. Since the Finslerian extension of a given Riemannian spacetime possesses a smaller symmetry than the original Riemannian spacetime [36,37], Finsler geometry is employed to elucidate some fundamental theories, such as the violation of Lorentz invariance [38–42], the anisotropy of the Universe, etc. [43–49]. In 1993, Rutz extended the vacuum field equations of general relativity to Finsler spacetime, resulting in the derivation of Finslerian gravitational field equations [50]. Given the preservation of symmetry in Finsler spacetime, the axially symmetric Finslerian extension of a Schwarzschild solution can be derived as a non-Riemannian exact solution to the vacuum field equation in Finsler geometry [51]. In order to maintain clarity in this paper, we will refer to this type of black hole as the Finslerian Schwarzschild black hole for short in following of the paper. Then, the Finsler Reissner-Nordström solution was derived, which is asymptotic to the Finsler spacetime with normal flag curvature at infinity [52]. Based on the study of the quasinormal modes of a scalar and an electromagnetic field in Finslerian Schwarzschild spacetime, it is found that the spherical symmetry of the black hole is broken, and the axial symmetry is displayed [53], a phenomenon also observed in Finsler Reissner-Nordstrom spacetime [54]. Additionally, the orbits of the Finslerian Schwarzschild black hole have been tested and constrained by the astronomical observation data [55]. The shadow of a black hole harbors copious amounts of information. As a universal approach for exploring the properties of spacetime, the primary objective of this work is to comprehend the structural characteristics of Finsler spacetime from the perspective of shadow. In the context of Finslerian Schwarzschild spacetime, we examine the geodesic motion of photon surrounding a black hole and explore the apparent shadow of the black hole that can be obtained by the observer. In addition, the photon trajectory near the Finslerian Schwarzschild black hole is numerically simulated with the different observation angles and Finsler parameter $\epsilon$. In particular, we expect to gain profound insights into the geometric structure of the Finsler spacetime and effectively differentiate it from the Schwarzschild case.

The remainder of the present paper is outlined as follows. In Sec. II, we will provide a brief introduction to Finslerian Schwarzschild spacetime and investigate the photon motions on this spacetime. In Sec. III, the celestial coordinates of distant observers are established in the Finslerian Schwarzschild spacetime. The apparent position and shape of the black hole shadow in the sky plane of the observer are studied under different Finsler parameter $\epsilon$ and observation inclinations $\theta_o$. Section IV ends with a brief discussion and conclusion.

## II. BRIEF INTRODUCTION OF THE FINSLERIAN SCHWARZSCHILD BLACK HOLE AND ITS PHOTON MOTIONS

As a natural extension of Riemann geometry, Finsler geometry liberates itself from the quadratic constraint on the form of metric [35]. In contrast to Riemann geometry, where the inner product is solely defined on the tangent bundle, Finsler geometry defines its inner product based on the unique Finsler structure $F$. When $\lambda > 0$, the Finsler structure $F$ demonstrates the remarkable property that $F(x, \lambda y) = \lambda F(x, y)$, in which $x \in \mathcal{M}$ represents position ($\mathcal{M}$ is the Finsler manifold), and $y \equiv dx/d\tau$ represents velocity ($\tau$ is the proper time), respectively. The Finslerian metric can be described as [35]

$$g_{\mu\nu} \equiv \frac{\partial}{\partial y^\mu}\frac{\partial}{\partial y^\nu}\left(\frac{1}{2}F^2\right). \tag{1}$$

The Finslerian spacetime can be characterized by the Finsler structure $F$, which is not positive definite at every point of the Finsler manifold. The causal structure of Finsler spacetime is determined by $F^2$, and in the case where it is quadratic in $y$, the Finslerian metric reduces to a Riemannian metric. When $F$ assumes a positive, zero, or negative value, it corresponds to spacelike curves, null, or timelike curves, respectively. As stated in [50], the vacuum field equation of Finslerian gravity is characterized by the vanishing of the Ricci scalar ($\mathrm{Ric} = 0$) and is shown as

$$\mathrm{Ric} = \frac{1}{F^2}\left(2\frac{\partial G^\mu}{\partial x^\mu} - y^\lambda \frac{\partial^2 G^\mu}{\partial x^\lambda \partial y^\mu} + 2G^\lambda \frac{\partial^2 G^\mu}{\partial y^\lambda \partial y^\mu} - \frac{\partial G^\mu}{\partial y^\lambda}\frac{\partial G^\lambda}{\partial y^\mu}\right). \tag{2}$$

Here, $G^\mu$ is geodesic spray coefficients, expressed as

$$G^\mu = \frac{1}{4} g^{\mu\nu} \left( \frac{\partial^2 F^2}{\partial x^\lambda \partial y^\nu} y^\lambda - \frac{\partial F^2}{\partial x^\nu} \right). \tag{3}$$

Here, we must point out that there are various generalizations of Einsteins gravitational field equations in Finslerian gravity, and the vacuum field equation proposed in Ref. [50] cannot be derived through an action principle [56]. In [51], a Finslerian Schwarzschild solution was derived from the Finslerian gravitational field equations, which distinguishes itself from the Schwarzschild solution in a two-dimensional subspace. The modified form of this solution, with geometrized units ($G = c = 1$), is as follows:

$$F^2 = -f(r) y^t y^t + f(r)^{-1} y^r y^r + r^2 \bar{F}^2, \tag{4}$$

in which

$$f(r) = 1 - \frac{2M}{r}. \tag{5}$$

In the above, $M$ is the mass of the black hole, while $\bar{F}$ represents a two-dimensional Finsler space endowed with positive constant flag curvature. One of the major differences between Riemannian geometry and Finsler geometry is that Finsler spaces with constant flag curvature are not equivalent to each other. In this work, we contemplate a Finsler space $\bar{F}$ that takes on the following configuration [51]:

$$\bar{F} = \frac{\sqrt{(1-\epsilon^2 \sin^2\theta) y^\theta y^\theta + \sin^2\theta y^\varphi y^\varphi} - \epsilon \sin^2\theta y^\varphi}{1 - \epsilon^2 \sin^2\theta}. \tag{6}$$

$\bar{F}$ introduces a departure from spherical symmetry while preserving axial symmetry. This characteristic has already been verified in the extended black hole within this two-dimensional Finsler space through the quasinormal modes [53,54]. The term $\epsilon$ represents the deformation parameter of Finsler space that characterizes the deviation between Finsler space $\bar{F}$ and Riemannian two-sphere, satisfying the condition $0 \leq \epsilon < 1$. It is evident that in the case of $\epsilon = 0$, the Finslerian Schwarzschild spacetime reverts back to Schwarzschild spacetime.

To scrutinize the motion behavior of photons near the Finslerian Schwarzschild black hole is imperative in order to analyze its shadow. As the Finsler structure $\bar{F}$ remains constant along the geodesic, and the motion of photons satisfies the Euler-Lagrangian equation [57], that is

$$\frac{d}{d\tau} \frac{\partial F^2}{\partial y^\mu} - \frac{\partial F^2}{\partial x^\mu} = 0. \tag{7}$$

The general form of geodesic equation is

$$\frac{d^2 x^\mu}{d\tau^2} + 2G^\mu = 0, \tag{8}$$

which preserves the Finsler structure. By exploiting the unique symmetry of Finslerian Schwarzschild spacetime [51], we can derive four constants of motion from the geodesic equation (8), which are

$$\dot{t} = \frac{E}{f(r)}, \tag{9}$$

$$\dot{r}^2 = E^2 - f(r) \frac{K^2}{r^2}, \tag{10}$$

$$\dot{\theta}^2 = \frac{K^2}{r^4} \frac{\sin^2\theta (K - \epsilon J)^2 - J^2}{\sin^2\theta (K - \epsilon J)^2}, \tag{11}$$

$$\dot{\varphi} = \frac{K}{r^2} \frac{\epsilon \sin^2\theta (K - \epsilon J) + J}{\sin^2\theta (K - \epsilon J)}. \tag{12}$$

Here, the overdot denotes differentiation with respect to the proper time $\tau$. The conserved quantities $E$ and $J$ come from the Killing vector of the Finslerian Schwarzschild black hole [51], representing the energy and angular momentum of the photon, respectively. The constant $K$ stems from geometric structure (6) of Finslerian Schwarzschild spacetime [55]. The behavior of photons in close proximity to the black hole can be analyzed utilizing Eqs. (9)–(12), thereby enabling a more specialized examination.

## III. SHADOW OF THE FINSLERIAN SCHWARZSCHILD BLACK HOLE FOR OBSERVERS AT INFINITE DISTANCE

The photon emitted from the source travels along the geodesic path as it passes near the black hole, and any photon absorbed by the black hole without reaching the observer's position creates a dark region in the sky plane of the observer, namely the black hole shadow. One can determine the apparent position of black hole shadow on the sky plane of the observer by introducing the following celestial coordinates [58–62]:

$$\alpha = \lim_{r_o \to \infty} \left( -r_o^2 \sin\theta_o \left. \frac{d\varphi}{dr} \right|_{(r=r_o, \theta=\theta_o)} \right), \tag{13}$$

$$\beta = \lim_{r_o \to \infty} r_o^2 \left. \frac{d\theta}{dr} \right|_{(r=r_o, \theta=\theta_o)}, \tag{14}$$

in which the term $r_o$ represents the distance between the observer and black hole, while $\theta_o$ denotes the inclination angle between the observer's sight line and the axis of black hole; see Fig. 1. Here, the coordinates $(\alpha, \beta)$ represent the apparent perpendicular distance of the image as seen from the axis of symmetry and the apparent perpendicular

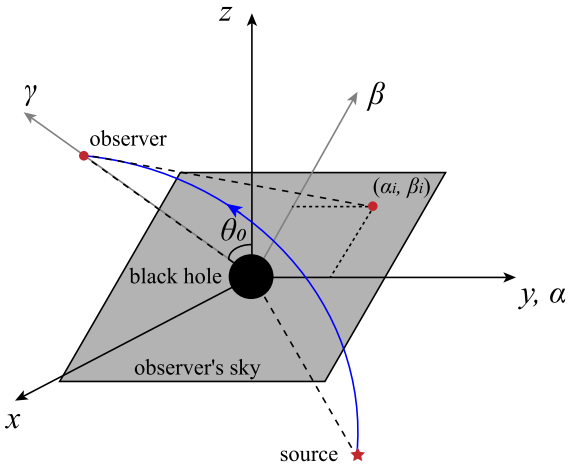


FIG. 1. The schematic representation of celestial coordinates, and the $\alpha-\beta$ plane is the observer's sky, in which the black sphere at the origin represents the black hole, and the blue line represents the light ray emitted from the source that can be received by the observer.

distance projected on the equatorial plane, respectively, and the line connecting the observer and the origin as the $\gamma-$ axis, with its positive direction as shown in Fig. 1. Without loss of generality, we can choose the $\varphi_o = 0$ so that the $y$ and $\alpha$ axis recombine.

Here, we must point out that the Finslerian Schwarzschild spacetime (4) does not approach Minkowski spacetime at infinity. The physical reasons why we choose the celestial coordinates (13) and (14) for the observers at infinity are listed as follows. In the local reference frame of an observer, the Lorentz violation in the vicinity of Earth is considered to be approximately negligible, thereby preserving the Minkowski spacetime property in close proximity to Earth [63]. In astrophysics, the measurement of celestial positions and angles primarily relies on the application of spherical trigonometry, which also serves as a crucial scientific tool in astronomical observation [64,65]. In the context of Finslerian Schwarzschild spacetime, Eqs. (13) and (14) can be reduced by utilizing the null geodesic Eqs. (10)–(12), which yield

$$\alpha_{\mathrm{FS}} = -\frac{\epsilon K(K-\epsilon J)\sin^2\theta_o + KJ}{E\sin\theta_o(K-\epsilon J)}, \tag{15}$$

$$\beta_{\mathrm{FS}} = \pm\frac{K\sqrt{(K-\epsilon J)^2\sin^2\theta_o - J^2}}{E\sin\theta_o(K-\epsilon J)}. \tag{16}$$

Hence, Eqs. (15) and (16) play a crucial role in determining the apparent position of the Finsler-Schwarzschild black hole shadow in the sky plane of observer ($\alpha-\beta$ plane). By combining Eqs. (15) and (16), one can obtain that

$$\left(\alpha_{\mathrm{FS}} + \frac{\epsilon K\sin\theta_o}{E}\right)^2 + \beta_{\mathrm{FS}}^2 = \left(\frac{K}{E}\right)^2. \tag{17}$$

In practice, a closed curve divides the observed shape into two regions based on whether or not the optical geodesic intersects the event horizon of the black hole. This curve is called the apparent boundary or critical curve, and the inner region of the apparent boundary is defined as the black hole shadow. The critical curve ultimately converges at the location of photon sphere. By utilizing the condition for the position of the photon ring, where $(\dot{r}=0, \partial_r\dot{r}^2=0)$, we can derive

$$\frac{E^2}{1-2M/r} = \frac{K^2}{r^2}, \tag{18}$$

and

$$r = 3M. \tag{19}$$

From Eqs. (18) and (19), one can obtain $\frac{K}{E} = 3\sqrt{3}M$, which is useful for Eq. (17). It reveals that the shadow of the Finslerian Schwarzschild black hole that appears in the observer's sky is a circle with radius $r_{\mathrm{FS}} = 3\sqrt{3}M$ and its center at $(-\frac{\epsilon K\sin\theta_o}{E}, 0)$. Thus, one can find that the shape of the shadow of the Finslerian Schwarzschild black hole is the same as the one in the Schwarzschild black hole. The major difference between the shadow of the Finslerian Schwarzschild black hole and the Schwarzschild black hole comes from the center of shadow. In the following subsection, we will test this theoretical results from numerical approach.

### A. The observation position is located on the equatorial plane

Due to the reversibility of the light path, one can simulate the trajectories of light rays from the observer at infinity to the vicinity of the Finslerian Schwarzschild black hole within the framework of geometric optics, namely the backward ray-tracing code [59,60]. A significant amount of light rays are emitted from the observer and propagate in all directions, experiencing gravitational influence from the black hole as they traverse through spacetime. Some of the light that is extremely close to the black hole will be captured by the black hole, thereby giving rise to the formation of the black hole shadow. Hence, we are concerned with the light ray that can be received by the observer. During the process of conducting numerical simulations, we set the position of the observer at $r_o = 200M$, as $200M$ can be considered effectively infinite compared to the gravitational radius.

When the observed inclination is $\theta_o = \pi/2$, we numerically simulate the position of those observable light rays in the sky plane of observer $(\alpha_i, \beta_i)$ with different values of $\epsilon$;

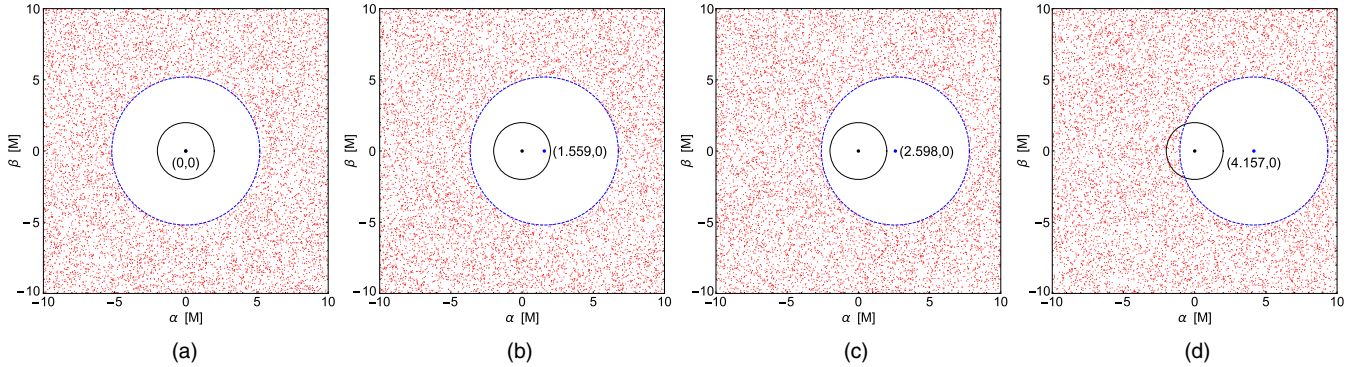


FIG. 2. The apparent shape of the shadow of the Finslerian Schwarzschild black hole on the sky plane of observer. Here, the solid line represents the location of event horizon, and the red dots indicate the point where the tangent line of light rays that can be received by the observer intersects the $\alpha-\beta$ plane. The blue and black dots represent the center of the shadow and the event horizon, respectively. (a) $\epsilon=0,\theta_o=\pi/2$, (b) $\epsilon=0.3,\theta_o=\pi/2$, (c) $\epsilon=0.5,\theta_o=\pi/2$, and (d) $\epsilon=0.8,\theta_o=\pi/2$.

see Fig. 2. Among them, the region without the red dot corresponds to the shadow region of the black hole, and we use the blue dashed line to numerically fit the outer boundary of the shadow region.

As the Finslerian parameter $\epsilon$ varies, one can find that the blue dashed line consistently manifests as a closed circle, indicating that the shadow shape of the Finslerian Schwarzschild black hole takes on a circular appearance in the observer's sky. This result aligns with Eq. (17), as it represents the mathematical expression of a circular shape. However, the apparent position of the black hole shadow undergoes a right shift along the horizontal axis, as the parameter $\epsilon$ increases. The value of $\epsilon$ is taken as $\epsilon=0$, 0.3, 0.5, 0.8, and the numerical coordinates of the apparent position (the location of the blue dot $X_C$) at the center of the shadow are (0, 0), (1.559, 0), (2.598, 0), and (4.157, 0), respectively. It shows that the coordinate position of the shadow center is positively correlated with parameter $\epsilon$, satisfying the relation $X_C\sim 5.20M\epsilon$, which also represents the distance the shadow moves on the horizontal axis. From these numerical results, it can be found that the relation between the coordinate position of the shadow center and the parameter $\epsilon$ corresponds to the theoretical position of the shadow center, i.e., $(-\frac{\epsilon K\sin\theta_o}{E},0)$, which is obtained in Eq. (17). It should be noted that the backward ray-tracing method is employed in our numerical calculations. The observed light rays are outputted in reverse, with the initial position being the observer's position $(r_o\to r_o,\theta_o\to\theta_o,\varphi_o\to 0)$, and the initial velocity being reversed $(\dot{r}_o\to-\dot{r}_o,\dot{\theta}_o\to-\dot{\theta}_o,\dot{\varphi}_o\to-\dot{\varphi}_o)$. As mentioned in [55], the Finsler space (6) is irreversible under $y^\varphi\to-y^\varphi$, meaning that the apparent position of black hole shadow moves to the opposite direction of Eq. (17).

For the different values of parameter $\epsilon$, the projection of numerical simulation of the trajectory of light emitted from the observer's position on the $\alpha-\gamma$ plane is shown in Fig. 3. The green line depicts the trajectory of light ray falling into the event horizon of the black hole, while the blue line represents the deflected light that can be detected by an observer. The red line corresponds to the critical curve, which plays a pivotal role in shaping the formation of the photon ring (the red circle). The red dot on each panel

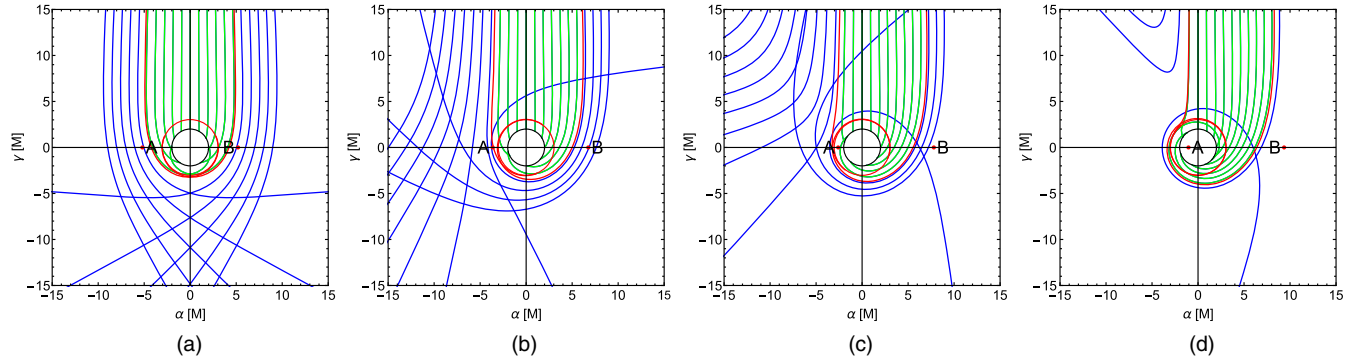


FIG. 3. The projection of trajectories of light rays in the vicinity of the Finslerian Schwarzschild black hole on $(\alpha-\gamma)$ plane with a different value of the Finsler paramater $\epsilon$, and the black and red circles represent the location of the event horizon and the photon ring, respectively. (a) $\epsilon=0,\theta_o=\pi/2$, (b) $\epsilon=0.3,\theta_o=\pi/2$, (c) $\epsilon=0.5,\theta_o=\pi/2$, and (d) $\epsilon=0.8,\theta_o=\pi/2$.

indicates the intersection of the tangent line of the critical ray along the observer's line of sight with the $\alpha-\beta$ plane, and the points corresponding to the forward and retrograde critical curves are denoted as $A$ and $B$, respectively. Actually, points $A$ and $B$ describe the position of the shadow cast by the black hole, and their distance $\overline{AB}$ is the diameter of the shadow. It can be found that the positions of points $A$ and $B$ will undergo a shift with respect to a variable parameter $\epsilon$, while the position of the photon ring remains unchanged. When the parameter $\epsilon$ is set to $\epsilon = 0$, 0.3, 0.5, 0.8, the numerical results of the distance between point $A$ and point $B$ are $\overline{AB} = 10.3903M, 10.3921M, 10.3934M, 10.3947M$. The results indicate that the numerical results of the diameter of the apparent shadow are consistent with the theoretical diameter of the shadow derived from Eq. (17), namely $\overline{AB} \sim 2r_{\mathrm{FS}} = 6\sqrt{3}M$. In addition, the position of point $A$ appears within the event horizon of the black hole if the parameter $\epsilon$ is set to a larger value ($\epsilon = 0.8$), resulting in the red dot within the event horizon as depicted in Fig. 2(d).

### B. The observation position is located on a nonequatorial plane

To gain a more comprehensive understanding of the geometry feature of Finslerian Schwarzschild spacetime, we expand the observer's position beyond the equatorial plane. In our setup, the radius coordinate $r_o$ of the observer is fixed as $r_o = 200M$, and the value of $\epsilon$ is taken as $\epsilon = 0.8$. When the position of the observer gradually moves from the equatorial plane of the black hole to the pole $0 < \theta_o < \pi/2$, we still give the position on observer's sky ($\alpha-\beta$ plane) of those rays that can be perceived by the observer, as shown in Fig. 4.

The result shows that the contour of the black hole shadow remains a spherical structure, and variations in the observer's inclination angle do not result in any distortion or alteration in the size of the black hole shadow. However, as the inclination angle decreases, the apparent position of the black hole shadow in the observer's sky gradually shifts from the right side of the plane to the left along the horizontal axis until it aligns with the center of the event horizon. The observation inclination is successively $\theta_o = \pi/2$, $\theta_o = \pi/3$, $\theta_o = \pi/6$, and $\theta_o = 0$, and the numerical coordinates of the apparent position at the center of the shadow are (4.157, 0), (3.602, 0), (2.087, 0), and (0, 0), respectively. It can be found that the coordinate position of the shadow center satisfies the relationship $X_C \sim 4.16M \sin\theta_o$, which closely aligns with the theoretical result $(-\frac{\epsilon K \sin\theta_o}{E}, 0)$ obtained in Eq. (17). In other words, the increase in the value of $\epsilon$ leads to a shift in the apparent position of the shadow, but this shift is gradually corrected by a decrease in the observed inclination.

The shadow in the case of $\epsilon = 0.8$ and $\theta_o = 0$ exhibits an apparent shape, size, and location that are similar to those in the Schwarzschild case ($\epsilon = 0, \theta_o = \pi/2$), that is, Figs. 2(a) and 4(d). In reality, the process of forming this visual similarity is fundamentally different, which will be illustrated in terms of photon trajectories. In Fig. 5, we show the projection of trajectory of light rays near the black hole on the $\alpha-\gamma$ plane at different observation angles. The observation angle of inclination decreases from left to right panels in the order of $\theta_o = \pi/2$, $\theta_o = \pi/3$, $\theta_o = \pi/6$, and $\theta_o = 0$ with the fixed parameter $\epsilon = 0.8$. It can be found that the decrease in observed inclination is accompanied by a gradual leftward shift of the shadow's position, i.e., the corresponding positions of red dots $A$ and $B$, along the horizontal axis until its center aligns with the center of the event horizon. For the case where the observation inclination are $\theta_o = \pi/2, \pi/3, \pi/6$, and 0, the numerical result of the distance between points $A$ and $B$ are $\overline{AB} = 10.3947M, 10.3934M, 10.3927M$, and $10.3905M$, respectively. The numerical results reveal that the distances of points $A$ and $B$ closely approximate $\overline{AB} \sim 6\sqrt{3}M$, which consistency aligns with the theoretical radius derived from equation (17). Comparing Figs. 5(d) and 3(a), it becomes

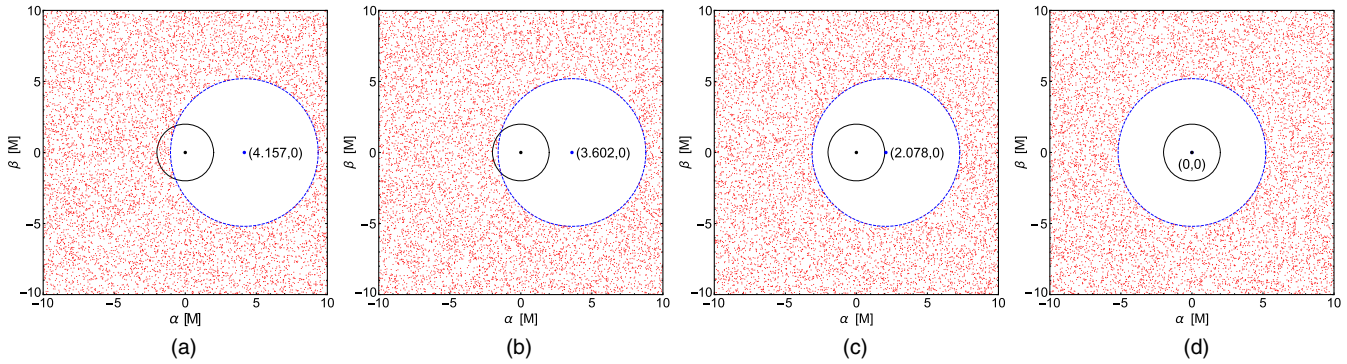


FIG. 4. The apparent shape of the shadow of the Finslerian Schwarzschild black hole in the observer's sky with different observation inclination. The black circle represents the location of the event horizons, while the red dots indicate where the tangent line of a light ray intersects with the observation plane and can be received by the observer. (a) $\epsilon = 0.8, \theta_o = \pi/2$, (b) $\epsilon = 0.8, \theta_o = \pi/3$, (c) $\epsilon = 0.8, \theta_o = \pi/6$, and (d) $\epsilon = 0.8, \theta_o = 0$.

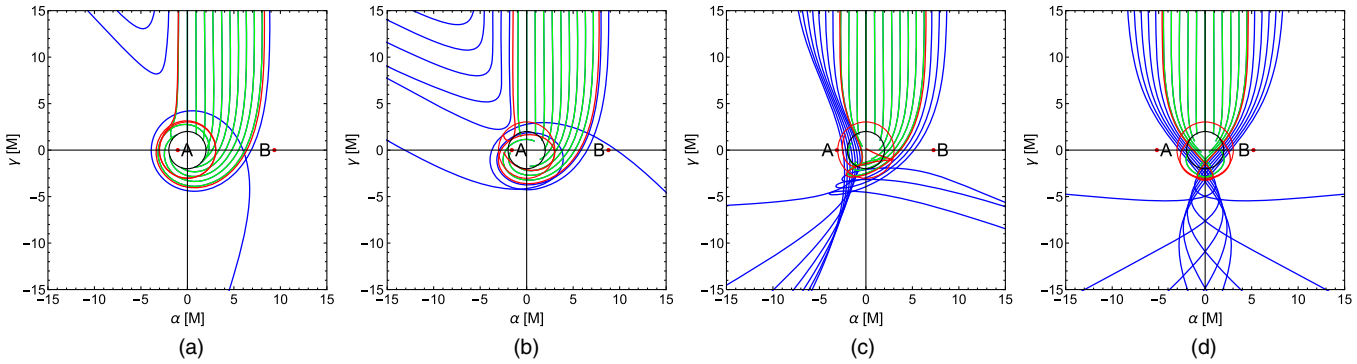


FIG. 5. The projection of trajectories of light rays in the vicinity of the Finslerian Schwarzschild black hole on $(\alpha-\gamma)$ plane with different observed inclination $\theta_o$, and the black and red circles represent the location of the event horizon and the photon ring, respectively. (a) $\epsilon=0.8,\theta_o=\pi/2$, (b) $\epsilon=0.8,\theta_o=\pi/3$, (c) $\epsilon=0.8,\theta_o=\pi/6$, and (d) $\epsilon=0.8,\theta_o=0$.

apparent that the trajectory of light in close proximity to the black hole is markedly distinct in both path and degree of deflection; although the apparent shape and position of their black hole shadows appear to be the same in the sky plane of observer, their spacetime structures are fundamentally dissimilar. In addition, the curvature of spacetime caused part of rays in Fig. 5(a) and in Fig. 5(b) to undergo severe deflection, and the tangents of these rays that intersect with the $\alpha-\beta$ plane are inside the event horizon, resulting in the presence of red dots within the event horizon region that correspond to Figs. 4(a) and 4(b).

In Fig. 5, it seems that some light rays pass through the event horizon of the black hole and are received by the observer. This phenomenon also occurs in Figs. 2(d), 4(a), and 4(b). The Finslerian Schwarzschild black hole does not allow the light rays to travel through the event horizon. Therefore, such phenomena should stem from the visual image of the light rays that were observed by the observer, which is located on coordinate $(\alpha,\beta)$ (13), (14). To accurately depict this phenomenon, the three-dimensional diagram illustrating the photon's trajectory can be employed; see Fig. 6. The blue lines depict light rays that are detectable by the observer, and the green lines illustrate light rays captured by the black hole, while the red lines represent the critical curve forming the photon sphere. As can be seen from Fig. 6, some light rays exhibit extreme deflection behavior near the black hole for the parameter $\epsilon$ is taken to a larger value, resulting in these light ray tracks crossing the event horizon when projected on the $\alpha-\gamma$ plane, which relate to Figs. 5(c) and 5(d). Therefore, the light ray passing through the event horizon of the black hole is a result of its trajectory being projected onto a specific plane, rather than representing the actual path of light crossing the event horizon. To a distant observer, the representational appearance of the black hole shadow obtained in Figs. 6(a) and 6(d) is almost indistinguishable, and the apparent position of the shadow in the sky plane of observer remains unchanged. However, the geometric structure of Finslerian Schwarzschild spacetime depicted in Fig. 6(d) exhibits a higher degree of complexity compared to the Schwarzschild case, resulting in the photon motion appearing richer and the degree of deflection being greater.

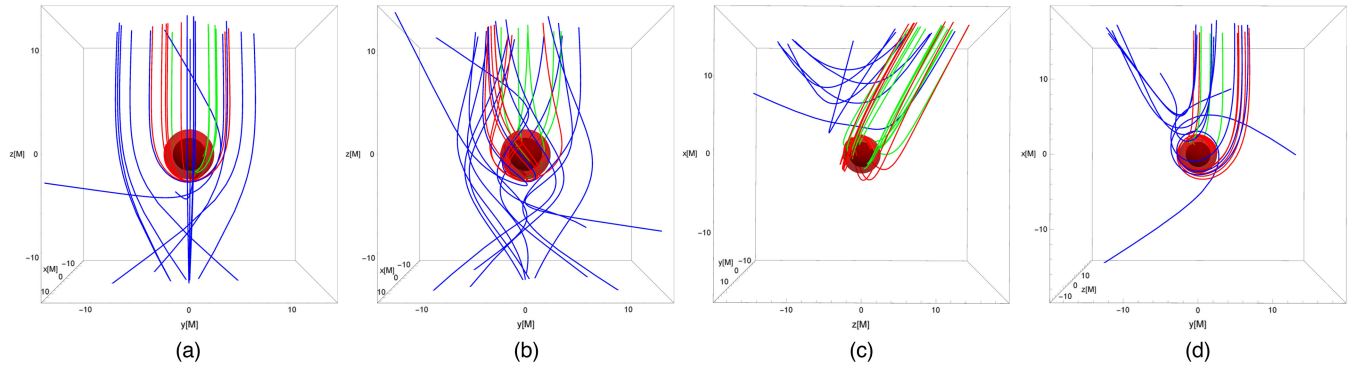


FIG. 6. The three-dimensional representation of the trajectory of light in close proximity to the Finslerian Schwarzschild black hole under the different observed inclination $\theta_o$ or Finsler parameter $\epsilon$, in which the black ball symbolizes the black hole, while the surrounding red region indicates the location of photon sphere. (a) $\epsilon=0,\theta_o=0$, (b) $\epsilon=0.8,\theta_o=0$, (c) $\epsilon=0.8,\theta_o=\pi/3$, and (d) $\epsilon=0.8,\theta_o=\pi/2$.

## IV. CONCLUSIONS AND DISCUSSIONS

In Finslerian Schwarzschild spacetime (4), we have investigated the characteristics of the apparent position and shape of a black hole shadow in the observer's sky. Additionally, we also numerically simulate the trajectory of light near black holes under different Finsler parameter $\epsilon$ and observation inclination angles $\theta_o$. To ascertain the apparent position and shape of shadow in the observer's sky, one typically constructs the celestial coordinates $(\alpha, \beta)$ in the Finslerian Schwarzschild spacetime. With the aid of the condition that the position of imposed by photon ring, one can find that the celestial coordinates of Finslerian Schwarzschild black holes satisfy a circular equation with radius of $r_{\mathrm{FS}} = 3\sqrt{3}M$, and the center of the circle is located at $(-\frac{\epsilon K \sin\theta_o}{E}, 0)$.

By utilizing the ray-tracing method, one can computationally simulate the apparent position and shape of the black hole shadow in the observer's sky while varying the Finsler parameter $\epsilon$, with a fixed observation inclination angle of $\theta_o = \pi/2$. The observation indicates that an increase in the Finsler parameter $\epsilon$ results in a horizontal displacement of the apparent shadow position, while maintaining an unaltered apparent shape and size. This result shares certain similarities and distinctions with the shadow cast by a Kerr black hole [18,66], which also possesses axial symmetry. Specifically, as the dimensionless spin parameter $\chi$ of the Kerr black hole increases, the position of the shadow also exhibits a phenomenon of horizontal displacement akin to that observed in Finslerian Schwarzschild spacetime. However, its shape deviates from a perfect circle and tends toward a $D$-shaped configuration, contrasting with the result in Finslerian Schwarzschild spacetime. For $\epsilon = 0.8$, the position of the shadow has shifted a great distance to the right, and the left contour of the shadow even overlaps with the position of black hole in the observed plane. In this system, the photon trajectory is deflected to a large extent near the black hole, where the intersection of the tangential vector of the critical curve with the $(\alpha, \beta)$ plane is the apparent position of the shadow in the observer's sky. As the value of the parameter $\epsilon$ changes, its intersection position shifts horizontally, resulting in a corresponding shift in the apparent position of shadow in the observer's sky. In addition, the numerical results show that the shift distance of the apparent position of shadow is positively correlated with the Finsler parameter $\epsilon$, which corresponds to the position of the center of the circle.

Furthermore, we also explore the shadow characteristics of Finslerian Schwarzschild black holes at various observed positions. The Finsler parameter fixed at $\epsilon = 0.8$, the observer inclination angle gradually varies, transitioning from the equatorial plane ($\theta_o = \pi/2$) of the black hole toward its pole ($\theta_o = 0$). Interestingly, the movement of the apparent position of the shadow is restored with the decrease of the observed inclination. In the case of $\theta_o = 0$, the shape, radius, and position of the black hole shadow are nearly indistinguishable from those in the case where $\epsilon = 0$ (Schwarzschild case). This characteristic exhibits similarities to the shadows cast by a Kerr black hole. With a reduction in the observational inclination angle, the differentiation between the Kerr shadow and that of the Schwarzschild case becomes increasingly minimal. Likewise, at $\theta_0 = 0$, they exhibit a high degree of similarity that makes them nearly indistinguishable. However, the consistency in shadow appearance does not necessarily imply equivalence in spacetime structure between this case and Schwarzschild spacetime. The result shows that the motion behavior of photon in Finslerian Schwarzschild spacetime is more intricate, and the photon trajectory has a greater degree of deflection near the black hole than in Schwarzschild spacetime. Therefore, as a property of spacetime itself, the black hole shadow is determined by the geometric structure of spacetime, but it also reflects the characteristics of the geometric structure of spacetime, helping us to understand the intrinsic properties of Finslerian Schwarzschild spacetime more intensely.

The Finslerian Schwarzschild spacetime (4) does not approach to Minkowski spacetime at infinity. The astronomical measurement is the main reason why we choose the celestial coordinates (13) and (14) for the observers at infinity. It means that we choose a Minkowskian observer at infinity to observe the shadows of Finslerian Schwarzschild black hole. If future observations for shadow of axial symmetric black hole shadow show signs of the Finslerian black hole, it better use the measurement of Finsler geometry. Reference [67] has studied the gravitational lensing effect in Finsler spacetime in which it presents a definition of angles in an intrinsic Finslerian way. The physical consequences of using this definition of angles is an interesting subject to investigate in the future.

## ACKNOWLEDGMENTS

This work has been supported by the National Natural Science Fund of China (Grant No. 12275034).

[1] R. Penrose, Phys. Rev. Lett. **14**, 57 (1965).
[2] B. P. Abbott *et al.* (LIGO Scientific and Virgo Collaborations), Phys. Rev. Lett. **116**, 241103 (2016).
[3] B. P. Abbott *et al.* (LIGO Scientific and Virgo Collaborations), Phys. Rev. Lett. **116**, 241102 (2016).
[4] B. P. Abbott *et al.* (LIGO Scientific and Virgo Collaborations), Phys. Rev. Lett. **116**, 061102 (2016).
[5] K. Akiyama *et al.* (Event Horizon Telescope Collaboration), Astrophys. J. **875**, L1 (2019).
[6] K. Akiyama *et al.* (Event Horizon Telescope Collaboration), Astrophys. J. **875**, L2 (2019).
[7] K. Akiyama *et al.* (Event Horizon Telescope Collaboration), Astrophys. J. **875**, L3 (2019).
[8] K. Akiyama *et al.* (Event Horizon Telescope Collaboration), Astrophys. J. **875**, L4 (2019).
[9] K. Akiyama *et al.* (Event Horizon Telescope Collaboration), Astrophys. J. **875**, L5 (2019).
[10] K. Akiyama *et al.* (Event Horizon Telescope Collaboration), Astrophys. J. **875**, L6 (2019).
[11] K. Akiyama *et al.* (Event Horizon Telescope Collaboration), Astrophys. J. Lett. **930**, L12 (2022).
[12] K. Akiyama *et al.* (Event Horizon Telescope Collaboration), Astrophys. J. Lett. **930**, L13 (2022).
[13] K. Akiyama *et al.* (Event Horizon Telescope Collaboration), Astrophys. J. Lett. **930**, L14 (2022).
[14] K. Akiyama *et al.* (Event Horizon Telescope Collaboration), Astrophys. J. Lett. **930**, L15 (2022).
[15] K. Akiyama *et al.* (Event Horizon Telescope Collaboration), Astrophys. J. Lett. **930**, L16 (2022).
[16] K. Akiyama *et al.* (Event Horizon Telescope Collaboration), Astrophys. J. Lett. **930**, L17 (2022).
[17] J. L. Synge, Mon. Not. R. Astron. Soc. **131**, 463 (1966).
[18] J. M. Bardeen, Timelike and null geodesics in the Kerr metric, in *Black Holes* (Les Astres Occlus), edited by C. DeWitt and B. S. DeWitt (Gordon and Breach, New York, 1973), p. 215.
[19] J. M. Bardeen, W. H. Press, and S. A. Teukolsky, Astrophys. J. **178**, 347 (1972).
[20] Y. Huang, S. Chen, and J. Jing, Eur. Phys. J. C **76**, 594 (2016).
[21] P. V. P. Cunha, C. A. R. Herdeiro, and E. Radu, Phys. Rev. D **96**, 024039 (2017).
[22] M. Wang, S. Chen, and J. Jing, J. Cosmol. Astropart. Phys. 10 (2017) 051.
[23] Z. Chang and Q. H. Zhu, J. Cosmol. Astropart. Phys. 09 (2021) 003.
[24] H. Lu and H. D. Lyu, Phys. Rev. D **101**, 044059 (2020).
[25] S. W. Wei, Y. C. Zou, Y. X. Liu, and R. B. Mann, J. Cosmol. Astropart. Phys. 08 (2019) 030.
[26] M. Zhang and J. Jiang, Phys. Lett. B **816**, 136213 (2021).
[27] P. C. Li, M. Guo, and B. Chen, Phys. Rev. D **101**, 084041 (2020).
[28] S. Guo, G. R. Li, and E. W. Liang, Phys. Rev. D **105**, 023024 (2022).
[29] X. X. Zeng, K. J. He, and G. P. Li, Sci. China Phys. Mech. Astron. **65**, 290411 (2022).
[30] A. Grenzebach, V. Perlick, and C. Lämmerzahl, Phys. Rev. D **89**, 124004 (2014).
[31] Q. Gan, P. Wang, H. Wu, and H. Yang, Phys. Rev. D **104**, 024003 (2021).
[32] S. W. Wei and Y. X. Liu, J. Cosmol. Astropart. Phys. 11 (2013) 063.
[33] K. J. He, X. Zhang, and X. Li, Chin. Phys. C **46**, 075103 (2022).
[34] K. J. He, S. C. Tan, and G. P. Li, Eur. Phys. J. C **82**, 81 (2022).
[35] D. Bao, S. S. Chern, and Z. Shen, *An Introduction to Riemann-Finsler Geometry* (Springer Press, New York, 2000), pp. 1–96.
[36] H. C. Wang, J. Math. Sociol. **S1-22**, 5 (1947).
[37] X. Li and Z. Chang, Differ. Geom. Appl. **30**, 737 (2012).
[38] F. Girelli, S. Liberati, and L. Sindoni, Phys. Rev. D **75**, 064015 (2007).
[39] G. W. Gibbons, J. Gomis, and C. N. Pope, Phys. Rev. D **76**, 081701 (2007).
[40] Z. Chang and X. Li, Phys. Lett. B **663**, 103 (2008).
[41] A. Kostelecky, Phys. Lett. B **701**, 137 (2011).
[42] V. Alan Kostelecký, N. Russell, and R. Tso, Phys. Lett. B **716**, 470 (2012).
[43] A. P. Kouretsis, M. Stathakopoulos, and P. C. Stavrinos, Phys. Rev. D **79**, 104011 (2009).
[44] A. P. Kouretsis, M. Stathakopoulos, and P. C. Stavrinos, Phys. Rev. D **82**, 064035 (2010).
[45] X. Li, H. N. Lin, S. Wang, and Z. Chang, Eur. Phys. J. C **75**, 181 (2015).
[46] X. Li, S. Wang, and Z. Chang, Eur. Phys. J. C **75**, 260 (2015).
[47] X. Li and S. Wang, Eur. Phys. J. C **76**, 51 (2016).
[48] X. Li and H. N. Lin, Eur. Phys. J. C **77**, 316 (2017).
[49] M. Hohmann, C. Pfeifer, and N. Voicu, Universe **6**, 65 (2020).
[50] S. F. Rutz, Gen. Relativ. Gravit. **25**, 1139 (1993).
[51] X. Li and Z. Chang, Phys. Rev. D **90**, 064049 (2014).
[52] X. Li, Phys. Rev. D **98**, 084030 (2018).
[53] X. Li and S. P. Zhao, Phys. Rev. D **101**, 124012 (2020).
[54] T. Y. Li, S. P. Zhao, and X. Li, Phys. Rev. D **105**, 104042 (2022).
[55] X. Li, X. Zhang, and H. N. Lin, Phys. Rev. D **106**, 064043 (2022).
[56] M. Hohmann, C. Pfeifer, and N. Voicu, Phys. Rev. D **100**, 064035 (2019).
[57] Z. Shen, *Lectures on Finsler Geometry* (World Scientific, Singapore, 2001).
[58] S. E. Vazquez and E. P. Esteban, Nuovo Cimento Soc. Ital. Fis. **119B**, 489 (2004).
[59] A. Abdujabbarov, M. Amir, B. Ahmedov, and S. G. Ghosh, Phys. Rev. D **93**, 104004 (2016).
[60] A. Abdujabbarov, F. Atamurotov, Y. Kucukakca, B. Ahmedov, and U. Camci, Astrophys. Space Sci. **344**, 429 (2013).
[61] M. Guo, N. A. Obers, and H. Yan, Phys. Rev. D **98**, 084063 (2018).
[62] Y. Meng, X. M. Kuang, and Z. Y. Tang, Phys. Rev. D **106**, 064006 (2022).
[63] C. M. Will, Living Rev. Relativity **17**, 4 (2014).
[64] W. M. Smart and R. M. Green, *Spherical Astronomy* (Cambridge University Press, Cambridge, England, 1977).
[65] K. R. Lang, *Astrophysical Formulae: Space, Time, Matter and Cosmology* (Springer Press, New York, 2010).
[66] S. Chandrasekhar, *The Mathematical Theory of Black Holes* (Oxford University Press, Oxford, 1983).
[67] B. Shen, J. Geom. Phys. **194**, 104999 (2023).